Available online at www.sciencedirect.com
ScienceDirect
Icarus 196 (2008) 477–487
ICARUS
www.elsevier.com/locate/icarus

Experimental study of the effect of wind on the stability of water ice on Mars

J.D. Chittenden [a,b], V. Chevrier [a,*], L.A. Roe [c], K. Bryson [a], R. Pilgrim [a], D.W.G. Sears [a,b]

[a] *W.M. Keck Laboratory for Space Simulation, Arkansas Center for Space and Planetary Science, MUSE 202, University of Arkansas, Fayetteville, AR 72701, USA*
[b] *Department of Chemistry and Biochemistry, University of Arkansas, Fayetteville, AR 72701, USA*
[c] *Department of Mechanical Engineering, University of Arkansas, Fayetteville, AR 72701, USA*

Received 19 April 2007; revised 28 January 2008

Available online 4 March 2008

Abstract

We have studied the effect of wind velocity on the sublimation rate of pure water ice under martian conditions. Measurements were made for wind velocities ranging from 0.7 to 11.4 m s^{-1}, a typical range observed by the meteorological instruments on the surface of Mars, and at −15 °C a value typical of the daily high temperature for most of the year at the Pathfinder landing site. At this temperature, and for a low-humidity environment (relative humidity around 1%) sublimation rates increase following a linear trend of equation $E_S = 0.68 + 0.025V$ (E_S is the sublimation rate in mm h^{-1} and V is the wind speed in m s^{-1}). In high relative humidity (30–35%) atmospheres, the effect of wind velocity is negligible, and the sublimation rate remains nearly constant at 0.33 ± 0.04 mm h^{-1}. Pure forced convection theory did not provide a satisfying description of the data in terms of the range of values and their wind speed dependency. Therefore, a new semi-empirical expression for the sublimation rate that combines free and forced convection was developed using analogy with heat transfer models. Using this expression, sublimation rates of ice as a function of wind velocity for any temperature can be calculated. In general, temperature is more important that wind speed and atmospheric humidity in determining the rate of sublimation of ice on Mars.

Keywords: Mars; Ices; Mars, surface; Mars, atmosphere

1. Introduction

The stability of water on Mars is of high interest for its geological and astrobiological implications and for its importance to human exploration. If the thermodynamic stability of ice is well understood, recent observations show that metastable ice could exist in several low-latitude regions of Mars (Bandfield, 2007; Jakosky et al., 2005). The sublimation of ice is in this case the primary factor controlling the metastability of ice on Mars. Several parameters have been shown to strongly affect the sublimation rate, such as the temperature (Chevrier et al., 2007; Sears and Chittenden, 2005), or the presence of soil layers (Chevrier et al., 2007; Farmer, 1976; Hudson et al., 2007). Some studies have also suggested that wind may increase the sublimation rates of water ice or liquid on the surface of Mars (Hecht, 2002), although to date there are no experimental data on the subject.

Measurements of surface winds from martian landers are scarce. The first surface measurements came from the Viking landers, which provided data between 1976 and 1981 (Hess et al., 1977; Schofield et al., 1997). Average wind velocity data measured at the Viking sites range from 5–10 m s^{-1} (Hess et al., 1977), with occasional excursions to 25–30 m s^{-1} during dust devil episodes and local dust storms (Ryan et al., 1981). In addition to Viking, the Pathfinder lander was equipped with a windsock experiment, which returned surface wind speeds between 6.94 and 9.68 m s^{-1} (Schofield et al., 1997; Sullivan et al., 2000).

The General Circulation Model (GCM) can be also used to infer surface wind speeds where direct measurements do not exist (Zent et al., 1993). Information on winds can also be obtained by tracking upper atmosphere clouds by orbiting spacecraft (Wang and Ingersoll, 2003), the Hubble Space Telescope (Kaydash et al., 2006; Mischna et al., 1998). Observations agree well with the GCM (Murphy et al., 1990).

* Corresponding author. Fax: +1 479 575 7778.
E-mail address: vchevrie@uark.edu (V. Chevrier).

0019-1035/$ – see front matter
doi:10.1016/j.icarus.2008.01.016

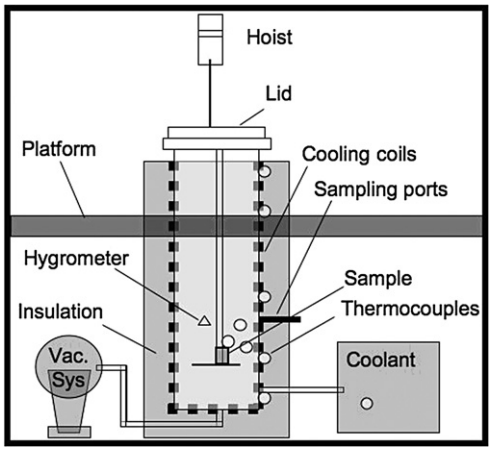

Fig. 1. Schematic diagram of the planetary simulation chamber used in these experiments. The 61 cm in diameter and 208 cm deep chamber is equipped with cooling system, vacuum system, thermocouples (shown as open circles) and hygrometer (shown as triangle).

Sears et al. (2005) showed that an increase in wind speed from 0 to 10 m s^{-1} would cause sublimation rate to increase by a factor of ten, assuming sublimation was governed by forced convection. Such increased was also shown by other studies (Hecht, 2002; Hisatake et al., 1993). In order to experimentally explore the influence of wind on the stability of water ice on Mars, we have performed laboratory experiments in which sublimation rates for pure water ice were determined under Mars conditions, using fans to create wind velocities up to ∼12 m s^{-1}.

2. Experimental set-up and methods

2.1. Experimental procedure

The planetary simulation chamber that was used in the present experiments has been described in previous papers (Chevrier et al., 2007; Sears and Chittenden, 2005; Sears and Moore, 2005) and is shown in Fig. 1. The equipment consists of a 0.6 m^3 stainless steel chamber, which is cooled to 0 °C using a Sterling SCMA-100 chilling system. Conditions in the chamber were monitored by eight thermocouples, a Pirani pressure gauge and a Rotronic hygrometer. To provide a simulated wind over the samples, two direct current fans were used, a 7.5 cm diameter Jamicon fan for wind speeds up to ∼4 m s^{-1} and an 11 cm diameter Mechatronics fan for wind speeds up to ∼12 m s^{-1}.

At the beginning of each experiment, the chamber was evacuated to less than 0.1 mbar, filled with 1 bar of dry CO_2 gas, and cooled to 0 °C. A sample consisting of a beaker with solid water ice level to the rim (prepared in a freezer at about −15 °C) was placed inside the chamber on a top loading analytical balance. The fan was then placed inside the chamber to simulate wind across the ice surface. The height of the fan was adjusted to obtain accurate and maximum wind velocity over the sample surface (Fig. 2, see next section for fan calibration). The chamber was closed and evacuated to 7 mbar (the process taking about 15–20 min). A period of 15–20 min was allowed for

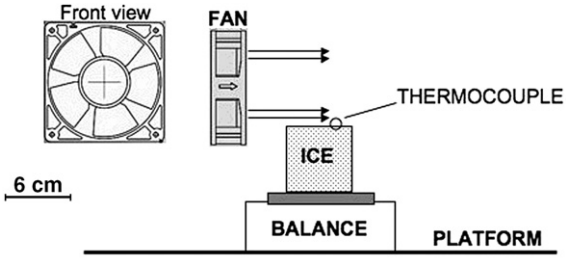

Fig. 2. Experimental set-up showing sample, balance, and fan. The placement of each is to scale.

the balance and analytical system to stabilize. Mass, humidity, pressure, and temperature (of the sample surface and the atmosphere) were logged every 15 s for 10 min at each wind velocity. The total atmospheric pressure was maintained between 6.5 and 7.5 mbar.

The experiments were run under two sets of atmospheric conditions, which we refer to as high and low relative atmosphere humidity (the atmospheric water vapor pressure relative to the saturation pressure of ice at the atmospheric temperature or p_{atm}/p_{sat}). In the high humidity case, atmospheric pressure was maintained at 7 mbar and the water vapor was allowed to build up inside the chamber during the experiment, so that the humidity typically reached ∼30%. In the low humidity case, the total pressure was maintained at 7 mbar but the chamber atmosphere was constantly exchanged with dry CO_2 gas to keep the humidity below ∼1%.

In the low relative humidity experiment, the temperature of the sample surface was initially 258 K (−15 °C, just out of the freezer) but increased during the pressure drop (probably because of warming by the still dense CO_2 atmosphere above) before dropping again to 258 ± 2 K where the temperature was maintained throughout the experiment (Fig. 3). The last effect results from evaporative cooling, and is discussed in detail in Section 4.2. Thus, all the results reported here were obtained at average temperatures of 258 ± 2 K for the sample surface and 273 K for the atmosphere. Similarly, the average surface temperature of the high humidity experiments is 263 ± 2 K for the same atmosphere temperature. All symbols presented in the following sections are summarized in Table 1.

2.2. Fan wind speed calibration

Prior to experiment, each fan was calibrated to relate to applied voltage to wind speed under martian conditions. The first step is to correlate the rotational speed of the fan with the speed of the wind, since the voltage applied controls only the rotational speed of the fan. The first fan law states that the volume of airflow rate is directly proportional to the fan rotational speed (McQuiston and Parker, 1982):

$$Q_2 = Q_1\left[\frac{\omega_2}{\omega_1}\right], \tag{1}$$

where Q is the volume flow rate, ω is the rotational speed of the fan, and subscripts 1 and 2 correspond to any two operating

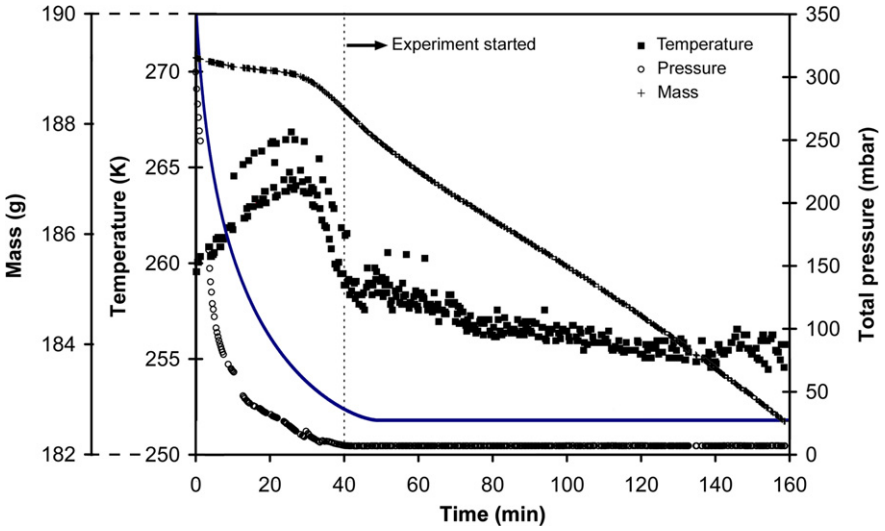

Fig. 3. Typical experimental run at zero wind speed showing various recorded data as a function of time, including mass (crosses), pressure (empty circles) and temperature (filled squares). The experiment starts as soon as the pressure reaches 7 mbar, when the sample starts to lose mass, which takes typically about 40 min. Simultaneously, the temperature of the surface starts to significantly decrease, as a result from the evaporative cooling effect (described in Section 4.2) and modeled here by the solid line, using Eqs. (10) and (13).

conditions. The wind speed V is defined as

$$V = \frac{Q}{A}, \tag{2}$$

where A is the area of the fan. Therefore, since A is constant the wind velocity can be correlated directly to the rotational speed of the fan:

$$V_2 = V_1\left[\frac{\omega_2}{\omega_1}\right]. \tag{3}$$

The rotational speed of the fan was determined with a Strobatac, a strobe light with a built-in frequency display. The strobe light frequency was adjusted until a white mark on the rotating fan appeared to stand still. The fan supply voltage was varied between 4 and 12 V in one-volt increments and the rotational speed ω recorded. Atmospheric (1000 mbar), 500 and 50 mbar pressures were investigated by use of a vacuum chamber equipped with windows. Fifty mbar was the lowest pressure reachable by this chamber. Therefore, rotational speeds had to be extrapolated to 7 mbar. For both fans we observe an increase of the rotational speed with decreasing pressure, at constant voltage (Fig. 4). This is due to the lower atmospheric density that reduces the drag on the fan blades. However, while the large fan speed versus voltage was better fit by linear regression, data from the smaller fan were better fit by second-order polynomial equations, probably because we reach the limits of the fan motor (Fig. 4). Using these regression lines at different pressure, we could extrapolate for each fan the rotational speed ω at 7 mbar as a function of the voltage applied to the fan. Then, using Eq. (4) and wind speed measured at ambient pressure (i.e. V_1 in Eq. (4)) we calculated the velocity of the wind at 7 mbar.

We then calculated the error on the wind speed extrapolated to martian conditions, using the following formula:

$$\frac{\Delta V_{7\text{ mbar}}}{V_{7\text{ mbar}}} = \sqrt{\left(\frac{\Delta u}{u}\right)^2 + \left(\frac{\Delta \omega}{\omega}\right)^2 + \left(\frac{\Delta V_m}{V_m}\right)^2}, \tag{4}$$

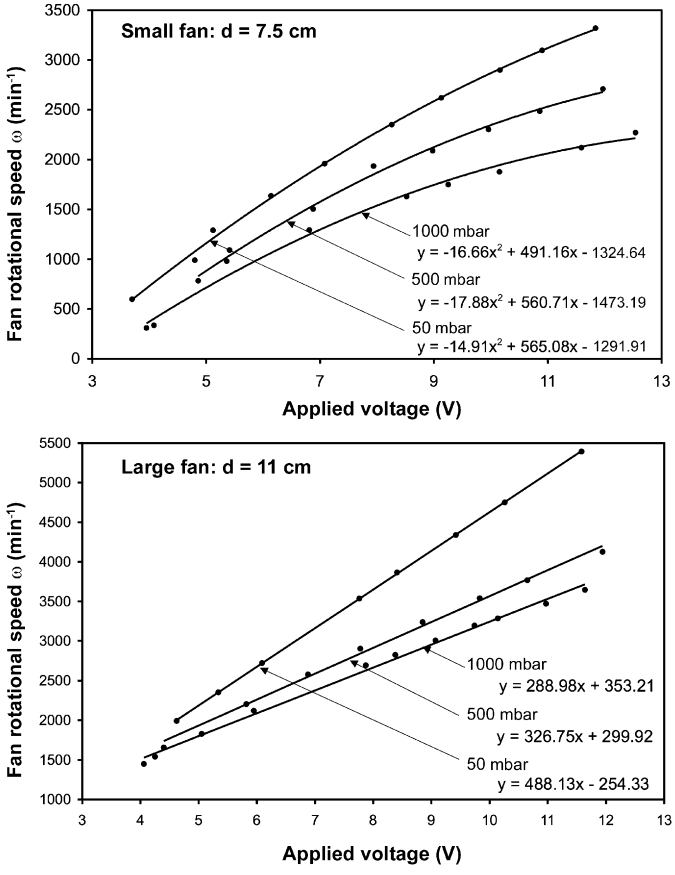

Fig. 4. Curves of rotational speed ω (in rotations per minute) of both fans used in these experiments as a function of the applied voltage. Also are represented the regression curves through the data, obtained at ambient pressure (1000 mbar), 500 and 50 mbar. Using these curves we can extrapolate the rotational speed of the fans at 7 mbar which is then converted into wind velocity using Eq. (3).

Table 1
Nomenclature of parameters used in this study

A	Cross-sectional area of the fan, m^2	Sc	Schmidt number, $Sc = \nu/D$
Cp	Specific heat, $J\,kg^{-1}\,K^{-1}$	Sh	Sherwood number, $Sh = E_S L_S/D$
d	Diameter of the fan, m	T_{atm}	Atmospheric temperature, K
D	Inter-diffusion coefficient of H_2O and CO_2, $m^2\,s^{-1}$	T_S	Surface temperature, K
D_{H_2O,CO_2}	Inter-diffusion coefficient of H_2O and CO_2, at standard conditions (273 K, 1 atm), $m^2\,s^{-1}$	u	Applied voltage, V
		V	Wind velocity, $m\,s^{-1}$
E_S	Sublimation rate, $m\,s^{-1}$ or $mm\,h^{-1}$	ΔC	Concentration difference, $mol\,m^{-3}$
g	Gravity constant, $m\,s^{-2}$	$\Delta\eta$	Relative water vapor density difference, $\Delta\eta = (\rho_{sat} - \rho)/\rho$
Gr	Grashof number, $Gr = (\Delta\rho/\rho)gL_G^3/\nu^2$		
J	Flux, $mol\,m^{-2}\,s^{-1}$	$\Delta H^S_{298\ K,1\ bar}$	Standard sublimation enthalpy, $J\,mol^{-1}$
L_G	Characteristic length in Grashof number, m	$\Delta\rho/\rho$	Relative gas ($CO_2 + H_2O$) density difference
L_R	Characteristic length in Reynolds number, m		
L_S	Characteristic length in Sherwood number, m	ΔT	Temperature difference, K
l	Thermal boundary layer in the ice, m	ν	Kinematic viscosity, $m^2\,s^{-1}$
P	Total atmospheric pressure, Pa	ρ_{atm}	Atmospheric water vapor density, $kg\,m^{-3}$
Q	Volumic flux of gas, $m^3\,s^{-1}$	ρ_{ice}	Water ice density, $kg\,m^{-3}$
Re	Reynolds number, $Re = VL_R/\nu$	ρ_{sat}	Water vapor saturation density, $kg\,m^{-3}$
Rh	Relative humidity, percent	ω	Rotational speed, s^{-1}

where $V_{7\ mbar}$ is the wind speed in martian conditions, V_m is the measured wind speed in ambient conditions (1 bar), and u is the voltage applied to the fan. We use the following errors for each parameter: $\Delta u = \pm 0.01$ V, $\Delta\omega = \pm 50\ min^{-1}$, and $\Delta V_m = \pm 0.1\ m\,s^{-1}$. Using these parameters, all errors fall in the range 0.10–0.14 $m\,s^{-1}$.

3. Results

Our data are presented in Table 2 and Fig. 5. The small gap in data at a wind velocity ~4 $m\,s^{-1}$ results from the transition from the 7.5 cm fan to the 11 cm fan.

For the low relative humidity experiments, we observe an increase in the sublimation rate with increasing wind speed. The average sublimation rate measured at zero wind speed is about $0.78 \pm 0.11\ mm\,h^{-1}$. The best fit of the low humidity data is obtained by a linear regression:

$$E_S = E_0 + KV \tag{5}$$

with V in $m\,s^{-1}$, E_S in $mm\,h^{-1}$, $E_0 = 0.68 \pm 0.01\ mm\,h^{-1}$ and $K = 0.025 \pm 0.002$. The value at zero wind speed extrapolated from the linear regression ($0.68 \pm 0.01\ mm\,h^{-1}$) is very close to the average value measured without the fan ($0.78 \pm 0.11\ mm\,h^{-1}$). Sublimation rates determined at 30% relative humidity do not show the same dependency with wind velocity as in a dry atmosphere. Moreover, the sublimation rates are lower than those measured in the low humidity experiments, on average $0.33 \pm 0.04\ mm\,h^{-1}$.

4. Discussion

4.1. Free convection and sublimation rate at zero wind speed

The sublimation rate of water ice is driven by a diffusion process from the surface to the atmosphere. From Fick's Law of diffusion we can determine the steady-state solution for the water vapor flux through any diffusive layer:

$$J = \Delta C \frac{D}{L}. \tag{6}$$

In general, ΔC is the concentration difference (in $mol\,m^{-3}$) across the diffusive barrier of thickness L, and D is the diffusion coefficient. Once converted into a sublimation rate E_S equation ($m\,s^{-1}$), the previous equation becomes:

$$E_S = \frac{D}{L}\Delta\eta. \tag{7}$$

In this case L is the thickness of the diffusive boundary layer on the surface of the ice, D is the diffusion coefficient of H_2O through CO_2, and $\Delta\eta$ is the water vapor concentration difference between the surface and the atmosphere, defined by

$$\Delta\eta = \frac{\rho_{sat} - \rho_{atm}}{\rho_{ice}}, \tag{8}$$

where ρ_{sat} is the saturation density of water vapor on the surface of the ice, ρ_{atm} is the density of water in the atmosphere (calculated from the relative humidity), ρ_{ice} is the ice density ($917\ kg\,m^{-3}$). Under conditions of free convection, the diffusion of water vapor from an icy surface is modified by the natural buoyancy of lighter water vapor moving through a heavier CO_2 atmosphere (Ingersoll, 1970). In those conditions, the diffusion equation is modified by the inclusion of the Grashof number Gr which is the ratio of buoyancy to viscous forces:

$$Gr = \left[\frac{(\Delta\rho/\rho)g}{\nu^2}\right] L_G^3, \tag{9}$$

where $(\Delta\rho/\rho)$ is the relative density difference of the gas mixture ($CO_2 + H_2O$) between the surface of the ice and the atmosphere, g is local gravitational acceleration, ν is the kinematic viscosity of CO_2, and L_G is a characteristic length for free convection. The corresponding sublimation rate is then calculated by the following equation (Ingersoll, 1970), where E_S is in $m\,s^{-1}$:

$$E_S = 0.17\Delta\eta D\left[\frac{(\Delta\rho/\rho)g}{\nu^2}\right]^{\frac{1}{3}}. \tag{10}$$

Table 2
Conditions and results of the present experiments[a]

Wind velocity ($m\,s^{-1}$)	T_S (K)	T_{atm} (K)	$Rh_{initial}$ (%)	Rh_{final} (%)	$E_S \pm \sigma$ ($mm\,h^{-1}$)
			Low humidity		
0.00	255	275	1.05	1.03	0.81 ± 0.11
0.00	256	274	1.12	1.06	0.84 ± 0.11
0.00	258	274	1.56	1.45	0.79 ± 0.11
0.00	258	275	0.61	0.56	0.93 ± 0.11
0.00	258	274	1.07	1.02	0.78 ± 0.11
0.00	262	274	2.22	2.09	0.80 ± 0.11
0.00	262	273	2.08	1.98	0.70 ± 0.11
0.00	257	274	0.50	0.47	0.85 ± 0.11
0.00	259	277	1.05	0.93	0.83 ± 0.11
0.00	258	275	0.89	0.82	0.58 ± 0.11
0.00	258	275	1.06	0.98	0.85 ± 0.11
0.00	258	275	0.95	0.90	0.91 ± 0.11
0.00	259	275	0.90	0.55	0.59 ± 0.11
0.00	258	274	1.03	0.98	0.80 ± 0.11
0.00	260	275	1.20	0.78	0.62 ± 0.11
0.67 ± 0.13	259	274	0.91	0.94	0.76 ± 0.13
0.67 ± 0.13	258	276	0.80	0.78	0.59 ± 0.13
0.82 ± 0.12	258	275	1.00	1.00	0.72 ± 0.05
0.82 ± 0.12	262	274	2.09	2.00	0.74 ± 0.05
0.82 ± 0.12	262	273	1.98	1.98	0.67 ± 0.05
0.82 ± 0.12	257	274	0.49	0.44	0.78 ± 0.05
1.06 ± 0.14	258	273	0.94	0.99	0.71 ± 0.09
1.06 ± 0.14	258	276	0.77	0.80	0.58 ± 0.09
1.25 ± 0.13	258	275	1.01	1.00	0.70 ± 0.04
1.25 ± 0.13	262	274	2.01	2.04	0.68 ± 0.04
1.25 ± 0.13	263	273	1.97	2.00	0.65 ± 0.04
1.25 ± 0.13	257	274	0.44	0.44	0.75 ± 0.04
1.42 ± 0.14	258	274	1.00	1.03	0.68 ± 0.05
1.42 ± 0.14	259	276	0.82	0.83	0.61 ± 0.05
1.65 ± 0.12	258	275	1.00	0.98	0.70 ± 0.03
1.65 ± 0.12	262	274	2.04	2.17	0.68 ± 0.03
1.65 ± 0.12	263	273	1.98	2.01	0.67 ± 0.03
1.65 ± 0.12	257	275	0.46	0.45	0.74 ± 0.03
1.76 ± 0.13	257	273	1.03	1.06	0.67 ± 0.03
1.76 ± 0.13	259	275	0.82	0.86	0.63 ± 0.03
2.03 ± 0.12	257	275	0.97	1.00	0.70 ± 0.02
2.03 ± 0.12	262	274	2.12	2.12	0.68 ± 0.02
2.03 ± 0.12	262	274	2.03	2.01	0.68 ± 0.02
2.03 ± 0.12	258	275	0.44	0.47	0.72 ± 0.02
2.07 ± 0.14	257	273	1.05	1.08	0.67 ± 0.03
2.07 ± 0.14	259	274	0.86	0.95	0.63 ± 0.03
2.36 ± 0.13	257	274	1.08	1.11	0.67 ± 0.02
2.36 ± 0.13	259	274	0.94	0.99	0.64 ± 0.02
2.37 ± 0.12	257	275	0.97	0.95	0.70 ± 0.02
2.37 ± 0.12	262	274	2.11	2.15	0.70 ± 0.02
2.37 ± 0.12	262	274	2.00	2.04	0.69 ± 0.02
2.37 ± 0.12	257	275	0.47	0.45	0.73 ± 0.02
2.62 ± 0.13	257	275	1.11	1.13	0.68 ± 0.01
2.62 ± 0.13	259	275	1.00	0.99	0.66 ± 0.01
2.69 ± 0.12	257	275	0.95	0.97	0.69 ± 0.01
2.69 ± 0.12	262	274	2.16	2.15	0.70 ± 0.01
2.69 ± 0.12	263	274	2.06	2.09	0.71 ± 0.01
2.69 ± 0.12	257	275	0.47	0.47	0.73 ± 0.01
2.85 ± 0.13	257	275	1.10	1.05	0.68 ± 0.01
2.85 ± 0.13	259	275	0.97	0.97	0.67 ± 0.01
2.98 ± 0.12	257	275	0.97	0.99	0.69 ± 0.02
2.98 ± 0.12	262	274	2.15	2.16	0.70 ± 0.02
2.98 ± 0.12	263	274	2.09	2.12	0.71 ± 0.02
2.98 ± 0.12	257	275	0.48	0.47	0.74 ± 0.02
3.06 ± 0.13	257	276	1.05	0.99	0.69 ± 0.02

(*continued in the next column*)

Table 2 (*continued*)

Wind velocity ($m\,s^{-1}$)	T_S (K)	T_{atm} (K)	$Rh_{initial}$ (%)	Rh_{final} (%)	$E_S \pm \sigma$ ($mm\,h^{-1}$)
3.06 ± 0.13	258	274	0.97	1.03	0.66 ± 0.02
3.24 ± 0.12	257	275	0.97	0.97	0.68 ± 0.03
3.24 ± 0.12	262	274	2.15	2.14	0.71 ± 0.03
3.24 ± 0.12	263	274	2.14	2.14	0.72 ± 0.03
3.24 ± 0.12	257	275	0.49	0.47	0.75 ± 0.03
3.47 ± 0.12	257	275	0.97	0.99	0.68 ± 0.03
3.47 ± 0.12	262	274	2.11	2.09	0.71 ± 0.03
3.47 ± 0.12	264	274	2.12	2.15	0.72 ± 0.03
3.47 ± 0.12	257	275	0.49	0.47	0.75 ± 0.03
3.99 ± 0.10	257	275	0.95	1.29	0.94 ± 0.18
3.99 ± 0.10	261	275	0.56	0.95	0.69 ± 0.18
4.27 ± 0.11	257	274	1.53	1.70	0.86 ± 0.08
4.27 ± 0.11	257	275	0.58	0.55	0.88 ± 0.08
4.27 ± 0.11	258	275	0.98	1.00	0.84 ± 0.08
4.27 ± 0.11	260	274	0.80	0.94	0.71 ± 0.08
4.35 ± 0.11	257	275	1.02	1.17	0.87 ± 0.10
4.91 ± 0.10	256	275	1.26	1.12	0.88 ± 0.13
4.91 ± 0.10	261	275	0.95	0.87	0.70 ± 0.13
5.28 ± 0.11	256	274	1.72	1.79	0.83 ± 0.07
5.28 ± 0.11	257	275	0.55	0.55	0.87 ± 0.07
5.28 ± 0.11	258	275	0.98	0.98	0.82 ± 0.07
5.28 ± 0.11	260	274	0.94	0.95	0.71 ± 0.07
5.32 ± 0.11	257	276	1.18	1.14	0.88 ± 0.10
5.82 ± 0.10	256	275	1.12	1.09	0.89 ± 0.11
5.82 ± 0.10	260	274	0.87	0.90	0.73 ± 0.11
6.29 ± 0.11	256	275	1.13	1.18	0.90 ± 0.10
6.30 ± 0.12	256	274	1.79	1.81	0.84 ± 0.06
6.30 ± 0.12	256	275	0.61	0.63	0.90 ± 0.06
6.30 ± 0.12	257	274	0.98	1.03	0.80 ± 0.06
6.30 ± 0.12	260	275	0.95	0.95	0.75 ± 0.06
6.74 ± 0.10	255	275	1.09	1.15	0.91 ± 0.10
6.74 ± 0.10	260	274	0.91	0.95	0.78 ± 0.10
7.25 ± 0.11	256	275	1.18	1.22	0.93 ± 0.10
7.32 ± 0.12	255	274	1.83	1.93	0.93 ± 0.07
7.32 ± 0.12	256	275	0.61	0.67	0.94 ± 0.07
7.32 ± 0.12	257	274	1.03	1.14	0.86 ± 0.07
7.32 ± 0.12	260	274	0.96	1.04	0.78 ± 0.07
7.65 ± 0.10	257	275	1.16	1.14	0.92 ± 0.07
7.65 ± 0.10	261	275	0.95	1.03	0.82 ± 0.07
8.22 ± 0.11	256	276	1.23	1.22	0.93 ± 0.07
8.33 ± 0.12	254	274	1.93	1.98	0.96 ± 0.07
8.33 ± 0.12	256	275	0.70	0.70	0.97 ± 0.07
8.33 ± 0.12	257	274	1.11	1.17	0.88 ± 0.07
8.33 ± 0.12	260	274	1.03	1.13	0.82 ± 0.07
8.57 ± 0.10	257	275	1.14	1.23	0.97 ± 0.06
8.57 ± 0.10	262	274	1.03	1.12	0.88 ± 0.06
9.18 ± 0.11	256	277	1.23	1.20	0.96 ± 0.10
9.35 ± 0.12	253	274	1.98	2.04	1.00 ± 0.08
9.35 ± 0.12	255	275	0.72	0.77	1.01 ± 0.08
9.35 ± 0.12	257	274	1.18	1.20	0.89 ± 0.08
9.35 ± 0.12	260	274	1.11	1.15	0.85 ± 0.08
9.48 ± 0.10	257	275	1.23	1.20	0.96 ± 0.07
9.48 ± 0.10	264	274	1.11	1.11	0.87 ± 0.07
10.15 ± 0.11	256	276	1.20	1.23	1.02 ± 0.10
10.37 ± 0.12	253	274	2.04	2.09	1.02 ± 0.09
10.37 ± 0.12	255	275	0.77	0.83	1.04 ± 0.09
10.37 ± 0.12	257	274	1.20	1.18	0.90 ± 0.09
10.37 ± 0.12	261	273	1.17	1.17	0.85 ± 0.09
10.40 ± 0.10	259	275	1.20	1.03	0.88 ± 0.05
10.40 ± 0.10	262	274	1.09	1.00	0.80 ± 0.05
11.12 ± 0.11	256	276	1.23	1.22	1.04 ± 0.10
11.39 ± 0.12	252	274	2.08	2.13	1.06 ± 0.11

(*continued on next page*)

Table 2 (*continued*)

Wind velocity ($m\,s^{-1}$)	T_S (K)	T_{atm} (K)	$Rh_{initial}$ (%)	Rh_{final} (%)	$E_S \pm \sigma$ ($mm\,h^{-1}$)
11.39 ± 0.12	256	276	0.81	0.83	1.08 ± 0.11
11.39 ± 0.12	259	274	1.20	1.23	0.93 ± 0.11
11.39 ± 0.12	262	274	1.17	1.23	0.86 ± 0.11
			High humidity		
0.00	261	276	15.65	17.04	0.40 ± 0.14
0.00	262	276	27.67	27.83	0.76 ± 0.14
0.00	261	273	18.01	21.01	0.31 ± 0.14
0.67 ± 0.13	261	275	17.10	18.35	0.43 ± 0.09
0.67 ± 0.13	263	276	27.84	28.70	0.31 ± 0.09
1.06 ± 0.14	261	274	18.53	20.20	0.38 ± 0.05
1.06 ± 0.14	263	275	28.76	30.70	0.30 ± 0.05
1.42 ± 0.14	261	273	20.37	22.06	0.39 ± 0.10
1.42 ± 0.14	264	275	30.79	32.93	0.26 ± 0.10
1.76 ± 0.13	261	273	22.26	23.99	0.34 ± 0.06
1.76 ± 0.13	264	275	32.97	33.66	0.26 ± 0.06
2.07 ± 0.14	261	273	24.12	25.53	0.30 ± 0.00
2.07 ± 0.14	265	275	33.69	34.88	0.30 ± 0.00
2.36 ± 0.13	262	274	25.66	26.78	0.31 ± 0.03
2.36 ± 0.13	265	275	34.93	36.30	0.27 ± 0.03
2.62 ± 0.13	262	274	26.83	27.67	0.33 ± 0.04
2.62 ± 0.13	265	276	36.27	36.39	0.26 ± 0.04
2.85 ± 0.13	262	274	27.75	28.65	0.30 ± 0.01
2.85 ± 0.13	265	277	36.39	35.15	0.32 ± 0.01
3.06 ± 0.13	262	274	28.67	29.96	0.28 ± 0.06
3.06 ± 0.13	265	276	35.11	36.37	0.36 ± 0.06
5.28 ± 0.12	261	274	20.76	22.41	0.35 ± 0.05
6.30 ± 0.12	261	274	22.53	24.65	0.33 ± 0.05
7.32 ± 0.12	262	273	24.77	27.13	0.32 ± 0.05
8.33 ± 0.12	263	273	27.16	29.31	0.31 ± 0.05
9.35 ± 0.12	263	274	29.35	30.26	0.34 ± 0.05
10.37 ± 0.12	263	274	33.49	33.19	0.36 ± 0.05
11.39 ± 0.12	264	275	33.18	33.32	0.33 ± 0.05

[a] Calculation of the uncertainty on the wind speed is described in Section 2.2. Uncertainty for temperature is 1 K, and uncertainty for relative humidity is 1%. Errors on the sublimation rates were determined for each experiment from the uncertainty on the slope of the regression line for the mass as a function of time.

This equation has been experimentally shown to give an accurate description of liquid water evaporation and ice sublimation in the absence of any forced convection (Moore and Sears, 2006; Sears and Chittenden, 2005; Sears and Moore, 2005). We calculate the diffusion coefficient D using the following formula (Boynton and Brattain, 1929):

$$D = D_{H_2O/CO_2}\left(\frac{T_{atm}}{273.15}\right)^{\frac{3}{2}}\left(\frac{10^5}{P}\right), \tag{11}$$

where D_{H_2O/CO_2} is the interdiffusion coefficient of H_2O and CO_2 ($1.387 \times 10^{-5}\ m^2\,s^{-1}$), T_{atm} is the atmospheric temperature, and P is the total atmospheric pressure (in Pa in this equation). The kinematic viscosity ν is determined from the Sutherland's formula (Crane, 1988):

$$\nu = 1.48 \times 10^{-5}\frac{RT_{atm}}{M_{CO_2}P}\left(\frac{240 + 293.15}{240 + T_{atm}}\right)\left(\frac{T_{atm}}{293.15}\right)^{\frac{3}{2}}, \tag{12}$$

where M_{CO_2} is the molecular mass of CO_2.

The sublimation rate at zero wind speed measured in this work in the low humidity experiments is $0.78 \pm 0.1\ mm\,h^{-1}$, or $0.68 \pm 0.01\ mm\,h^{-1}$ (extracted from the linear regression), so around $0.74\ mm\,h^{-1}$. This value is 4 times higher than the sublimation rate determined from Eq. (10) for ice at 258 K ($0.17\ mm\,h^{-1}$), and measured for liquid brines at low temperature (Sears and Chittenden, 2005). This effect is also observed in the case of the humid atmosphere, where the average sublimation rate is $0.33 \pm 0.04\ mm\,h^{-1}$ whereas Eq. (10) predicts 0.02–0.03 $mm\,h^{-1}$ at a surface temperature of 263 ± 2 K, i.e. a factor 10.

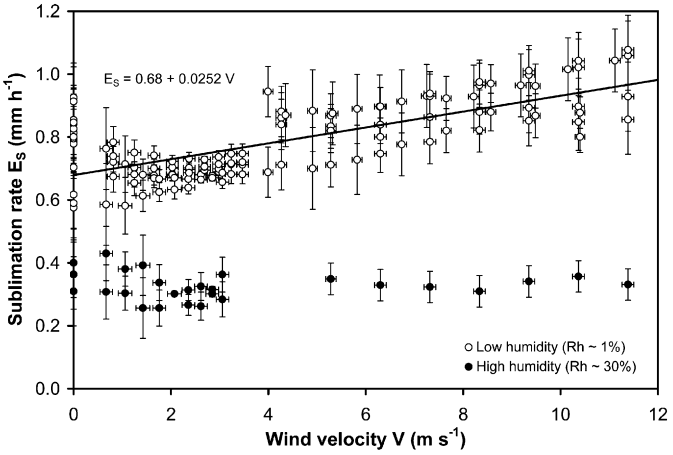

Fig. 5. Sublimation rate of ice as a function of the wind velocity, for a low-humidity (~1%, white circles) and a high humidity (~30%, black circles) atmosphere. The black line is a regression line through the low-humidity data.

Equation (10) applies perfectly when the surface of the ice and the atmosphere are at the same temperature. However, the situation gets more complicated when the surface and the atmosphere are at different temperatures. In order to input the right temperature in Eq. (10), two processes must be accounted for: (1) evaporative cooling of the ice which creates a temperature difference between the surface and the atmosphere, and (2) the resulting formation of a thermal boundary layer above the ice, which controls the diffusion and the buoyancy process.

4.2. Evaporative cooling of the ice surface

Each experiment in low-humidity atmosphere shows the same initial decrease of the ice surface temperature from the initial 273 K to about 258 ± 2 K. This results from evaporative cooling of the ice. Indeed, if the ice surface is thermodynamically unstable and thus spontaneously sublimates, it requires an energy source for the solid–gas phase transition. However, the thermal conductivity of the atmosphere (~0.02 $W\,m^{-1}\,K^{-1}$) is well below that of the ice (~2 $W\,m^{-1}\,K^{-1}$). Therefore, the molecular monolayer that sublimates takes the energy from the ice, rather than from the atmosphere. This results in a temperature decrease of the ice surface. We can verify the measured temperature on the surface of the ice by calculating the amount of energy necessary to sublimate the ice according to the sublimation rate at 273 K, and then the resulting decrease in temperature with time ($\partial T/\partial t$) using the simple following

Table 3
Typical values of parameters used in Eqs. (10) and (22) at various temperatures and for the humidity relevant to our experimental conditions

Temperature (K)	ρ_{sat} (kg m^{-3})	ρ_{atm} (kg m^{-3})	$\Delta\eta$	$\Delta\rho/\rho$	D (m^2 s^{-1})	ν (m^2 s^{-1})
			Low humidity (Rh < 1%)			
273[a]	4.84×10^{-3}	0.0	5.28×10^{-6}	1.06	1.98×10^{-3}	1.02×10^{-3}
268[b]	3.24×10^{-3}	0.0	3.53×10^{-6}	0.484	1.93×10^{-3}	1.00×10^{-3}
260[c]	1.98×10^{-3}	0.0	1.80×10^{-6}	0.144	1.84×10^{-3}	9.71×10^{-4}
			High humidity (Rh = 30%)			
273[a]	4.84×10^{-3}	1.59×10^{-3}	3.55×10^{-6}	0.714	1.98×10^{-3}	1.02×10^{-3}
268[b]	3.24×10^{-3}	1.62×10^{-3}	1.77×10^{-6}	0.234	1.93×10^{-3}	1.00×10^{-3}
263[c]	2.14×10^{-3}	1.65×10^{-3}	5.34×10^{-7}	2.53×10^{-3}	1.87×10^{-3}	9.82×10^{-4}

[a] Atmosphere temperature.
[b] Boundary layer temperature.
[c] Ice surface temperature.

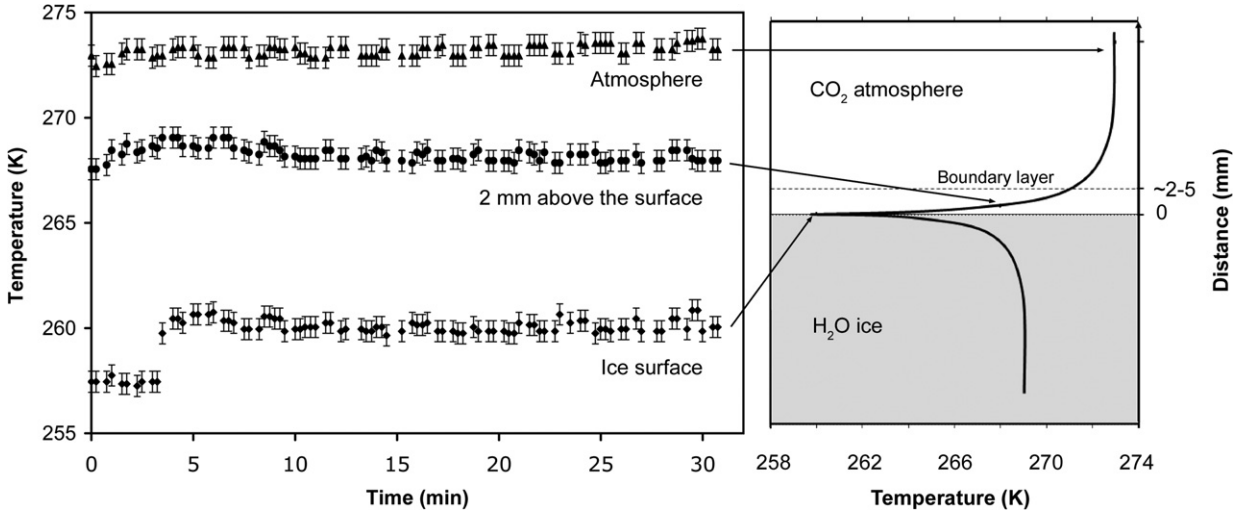

Fig. 6. Temperature as a function of time during an experiment, for three different positions: on the surface of the sample, 2 mm above the sample and in the atmosphere (left figure). The thermal boundary layer effect is schematized on the right figure, with temperature decreasing strongly in the boundary layer to reach the surface temperature. The data suggest that the boundary layer temperature, rather than the surface, controls the sublimation rate (see Section 4.3 for details).

thermodynamic equation:

$$\frac{\partial T}{\partial t} = \frac{E_S \Delta H^S_{298\ \mathrm{K},1\ \mathrm{bar}}}{l\mathrm{Cp}}, \tag{13}$$

where $\Delta H^S_{298\ \mathrm{K},1\ \mathrm{bar}}$ (51.059 kJ mol^{-1}) is the sublimation enthalpy of water ice (considered constant in the small 15–20 K temperature range), Cp (34.74 J mol^{-1} K^{-1}) is the specific heat of ice (both data from the CRC Handbook of Chemistry and Physics, CRC, 2005–2006) and l is the thickness of ice affected by the thermal change. We fixed the l value at 10 mm which is the typical order of magnitude of the thickness of our samples. According to Eq. (10), changes in l affect only how fast evaporative cooling is effective, but not the temperature of equilibrium, which depends only on the sublimation rate. We numerically solved Eq. (10) to determine the temperature profile. The result shows that the temperature decreases over the first 120 min, stabilizing around 252 K (Fig. 3). A similar calculation but with a 30% relative humidity gives a temperature drop to 262 K in about 60 min. This result is even closer to the measured surface temperature in the humid experiments, i.e. 263 ± 2 K. In the low-humidity experiments, the temperature decrease does not exceed 18 K (Fig. 3) since when the temperature difference becomes important, heat transfer from the atmosphere contributes to slightly warm the surface. Nevertheless, since the amplitude of the evaporative cooling effect is largely dependent on the sublimation rate and then in turn on the temperature, it should be negligible in the very low martian surface temperatures.

4.3. The thermal boundary layer effect

It is usually assumed that the ice surface temperature strongly controls the sublimation rate (Chevrier et al., 2007). However, Eq. (10) is for diffusion through the atmosphere, modified by the buoyancy term (Grashof number). Therefore, the temperature that should control the sublimation rate is the temperature of the boundary layer in which diffusion and buoyancy occur (frequently called the film layer) rather than the temperature of the ice surface. We ran a sublimation experiment in dry atmosphere, during which we measured the temperature of the ice surface, of the gas about 2 mm above the surface

and of the atmosphere (about 20 cm above the surface). The results (Fig. 6) show that while the atmosphere is at 273 K and the ice surface at 260 K, the gas layer just above the surface is at 268 K. The sublimation rate, as calculated from Eq. (10), is 0.73 mm h^{-1} at 268 K in a dry atmosphere, a value very close to the data at zero wind speed (0.68 to 0.78 mm h^{-1}). Similarly, in the case of the humid experiments, using a 268 K boundary layer temperature gives a sublimation rate of 0.25 mm h^{-1}, very close also to the measured value (0.33 mm h^{-1}). Therefore, the diffusion boundary layer controls the sublimation rate, and the relevant gas properties should be calculated at the boundary layer temperature rather than the ice surface temperature.

4.4. Previous work on forced convection

The previous equations are valid if there is no horizontal movement of the surrounding gas, or no atmospheric circulation. The boundary layer is, however, affected by the presence of wind, which forcibly removes water vapor away from the surface of the ice. The way wind modifies the boundary layer is characterized by the Reynolds number, i.e.:

$$Re = \frac{V L_R}{\nu}, \tag{14}$$

where V is the wind speed and L_R is a characteristic length for viscous effects, which, for our experiments, would be the diameter of the ice surface. Using our standard experimental conditions, i.e. $V \sim 10\ \mathrm{m\,s^{-1}}$ maximum (in our experiments and on Mars), $x \sim 10$ cm and $\nu \sim 10^{-3}\ \mathrm{m^2\,s^{-1}}$ (kinematic viscosity of CO_2 at 273 K, 700 Pa), we determine a Reynolds number $Re \sim 1000$. Under such conditions, the thickness of the boundary layer is defined by Hisatake et al. (1993):

$$L = \sqrt{\frac{\nu L_R}{v}}. \tag{15}$$

Hisatake et al. (1993) replaced L in Eq. (7) with this expression, giving the sublimation equation in the presence of horizontal flow:

$$E_S = \Delta\eta \frac{\rho_{\mathrm{atm}}}{\rho_{\mathrm{ice}}} D \sqrt{\frac{V}{\nu L_R}}. \tag{16}$$

Applying Eq. (16) to our conditions not only does not reproduce the data (linear dependence rather than square root of the wind speed) but it gives a sublimation rate about one order of magnitude higher than measured (Fig. 7). This is due to the fact that the boundary layer thickness associated with forced convection is much thinner than the buoyancy characteristic dimension (i.e. L_G in Grashof number in Eq. (9) is different from the boundary layer thickness L_R in Eq. (15)). It is not possible to simply "interchange" boundary layers in the case of the presence of wind. Therefore, a more complete model needs to be developed, accounting for both free and forced convection.

4.5. Mixed convection regime

Our data set falls in a regime where both free and forced convection (mixed convection) may be significant. Some heat

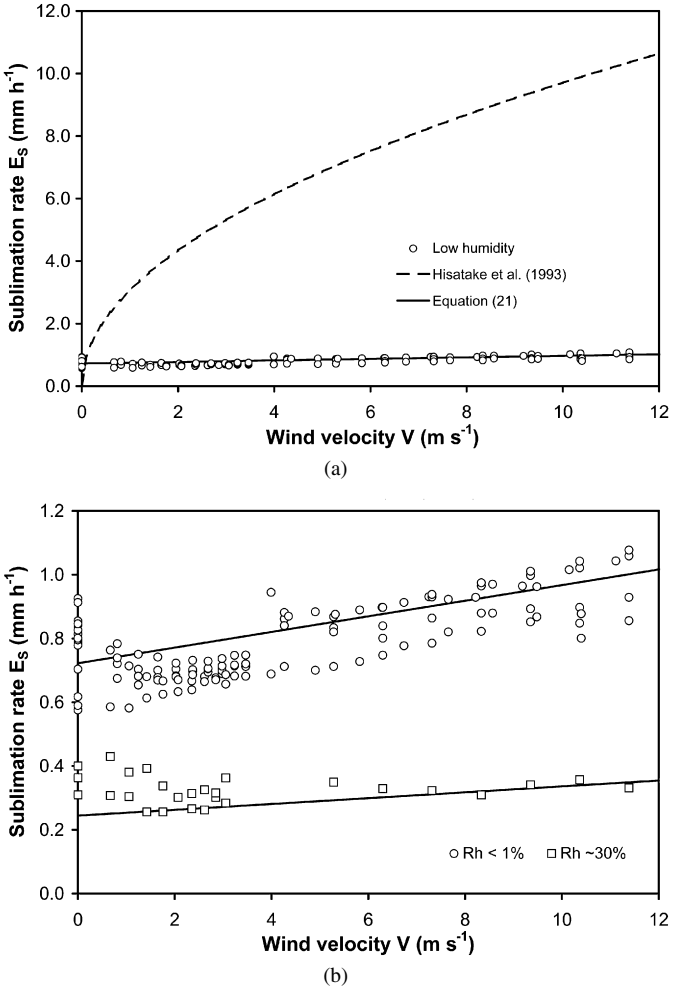

Fig. 7. (a) Comparison of the data with previous theories about sublimation/evaporation rates in the presence of forced convection using Eq. (16) from Hisatake et al. (1993). The solid line represents the fit obtained using Eq. (22). (b) Theoretical lines determined from Eq. (22) and applied to low (circles) and high (squares) humidity. Error bars have been removed for clarity but can be seen in Fig. 5. We used the temperature of the boundary layer, i.e. 268 K (see Sections 4.2 and 4.3 for more details). In both case, our theoretical equation provides a very satisfactory fit of the data.

transfer models for mixed convection involving wind have previously defined empirical equations extremely similar to our Eq. (5) such as the following (McAdams, 1954):

$$h = 5.7 + 3.8V, \tag{17}$$

where h is heat transfer coefficient (analogous to D in Eq. (7)) and V is the wind speed. This equation has been used to describe convective heat transfer between the atmosphere and ground in permafrost simulations (Zarling and Braley, 1988). For fixed driving force (temperature difference for heat transfer, concentration difference for mass transfer) both Eqs. (17) and (5) exhibit the characteristic that the transfer rate is equal to a free convective term (buoyancy driven, no velocity) plus a forced convective term that is linearly proportional to V.

There is often a strong similarity between heat and mass transfer semi-empirical models, and this is apparent from the nondimensional numbers describing the physics of the prob-

lems: the Sherwood number in mass transfer is equivalent to the Nusselt number in heat transfer while the Schmidt number in mass transfer is equivalent to the Prandtl number in heat transfer (see below for the definition of the Sherwood and Schmidt numbers). Equation (10) is also built on the analogy between mass and heat transfer (Ingersoll, 1970). Moreover, we have demonstrated in Sections 4.2 and 4.3 the strong coupling between heat and mass transfer, especially in the boundary layer. Therefore, using as a basis the empirical equation (5), Eq. (7) and several previously developed analogies with heat transfer (Arpaci and Kao, 2001; Churchill and Chu, 1975; Popiel and Wojtkowiak, 2004), we redefine the general nondimensional equation for ice sublimation by including separate terms for free convection (buoyancy) and forced convection (wind):

$$Sh = \Delta\eta \frac{\rho_{\text{atm}}}{\rho_{\text{ice}}} \left[k_1 Gr^{m_1} + k_2 Re^{n_1} Sc^{n_2} \right], \tag{18}$$

where Sh is the Sherwood number, which describes the global transfer of matter:

$$Sh = \frac{E_S L_S}{D}, \tag{19}$$

where L_S is a characteristic dimension for the global mass transfer process, and Sc is the Schmidt number:

$$Sc = \frac{\nu}{D}. \tag{20}$$

k_1 and k_2 are two constants (usually adapted to the data) and m_1, n_1, n_2 are three exponents, usually present in the semi-empirical equations (such equations are rarely linear functions of the nondimensional numbers). To match the previously verified free convection solution Eq. (10), $m_1 = 1/3$ and $k_1 = 0.17$, assuming $L_G = L_S$.

For forced convective heat transfer, relationships among Re, Nu and Pr usually take the form $Nu = CRe^{n1} Pr^{n2}$. This relationship is derivable from boundary layer theory for laminar flows (Schlichting, 1968). Because this relationship is of a convenient form (which can, in fact, be derived for more complex flow and temperature fields), it is often used for other geometries and turbulent flows. In those cases, the constants C, n_1, and n_2 are often determined empirically. The Reynolds number exponent, n_1, typically ranges from 0.5 to 1.0, while the Prandtl number (Pr) exponent is usually between 0.25 and 0.5 (Kays and Crawford, 1980; McAdams, 1954; Schlichting, 1968). Our data (Eq. (5)) and Eq. (17) suggest that the dependency is linear with wind speed, so that $n_1 = 1$. Although we confess the absence of data to verify this part of the equation, by analogy with heat transfer models, we assume that the Schmidt number has an exponent $n_2 = 1/3$. If we then assume that $L_S = L_G = L_R$, and using the values of ν and D at 268 K, we determine $k_2 = 1.23 \pm 0.3 \times 10^{-3}$. Therefore, we can rewrite Eq. (18) as

$$Sh = \Delta\eta \frac{\rho_{\text{atm}}}{\rho_{\text{ice}}} \left[0.17 Gr^{\frac{1}{3}} + 1.23 \times 10^{-3} Re\, Sc^{\frac{1}{3}} \right]. \tag{21}$$

In its dimensional form, Eq. (21) becomes:

$$E_S = \Delta\eta \frac{\rho_{\text{atm}}}{\rho_{\text{ice}}} \left(\frac{D}{\nu} \right)^{\frac{2}{3}} \left[0.17 \left(D \frac{\Delta\rho}{\rho} g \right)^{\frac{1}{3}} + 1.23 \times 10^{-3} V \right]. \tag{22}$$

In this equation, V and E_S are in m s^{-1}. Even if highly hypothetical, and requiring more experimental verification, this equation allows extrapolating the sublimation rate at various temperatures and wind velocities. The theoretical line from Eq. (22) is presented in Fig. 7b, being very similar to the regression line on the data (Eq. (5), Fig. 5), as expected since we used our data to derive the coefficients in Eq. (22). Note also that assumptions related to the characteristic lengths are only necessary to formulate the nondimensional form, Eq. (21), and none of these lengths (L_S, L_G, L_R), or any of the assumptions regarding them, affect the development of Eq. (22). It is also expected that the sublimation rate will not, in general, be a function of the dimensions of a flat sublimating surface, so the absence of length terms in Eq. (22) is to be expected. Finally, we observed earlier that experiments performed in high humidity atmosphere (Rh $\sim$ 30%) did not show any dependency of the sublimation rate with wind speed within the error bars. In fact, this is because at higher humidity, the effect of wind is even smaller. Thus our data at higher humidity have too much scatter and large error bars to show the very small slope of the theoretical line (Fig. 7b). This provides nevertheless an excellent and independent verification of the validity of our theoretical treatment of the wind effect on the sublimation rate of water ice in martian conditions.

4.6. Stability of ice on Mars

Hecht (2002) pointed out that wind velocities greater than 2.37 m s^{-1} on Mars (equivalent to 3.84 m s^{-1} on Earth) caused a considerable increase in sublimation rate and that in order to minimize heat loss and make liquid water on the surface feasible wind speeds below this value are required. The present data suggest that the effect of wind may be less significant than previously assumed for Mars. This is nevertheless true for a constant humidity between the wind and the atmosphere above the ice surface. If some "dry" wind is blowing above ice, the effect of wind will be increased mostly because of removal of water vapor (similar in a way to evaporating in dry atmosphere), but our results show that the sheer effect of wind is not very important. In fact, the main parameter controlling the sublimation rate of ice remains the surface temperature (Fig. 8a), which changes the sublimation rate by 8–9 orders of magnitude over the temperature range of the martian surface.

The effect of wind speed becomes more important at lower temperature, so that while the variation in sublimation rate for wind speed ranging from 0 to 14 m s^{-1} is only about a factor 1.5 at 268 K, it changes by 2 orders of magnitude at 170 K (Fig. 8b). Therefore, colder regions, while globally more stable, may experience wider variations of sublimation rate than warmer regions.

It is established that ice is not stable on the surface of Mars in equatorial regions. However, metastable ice could be present

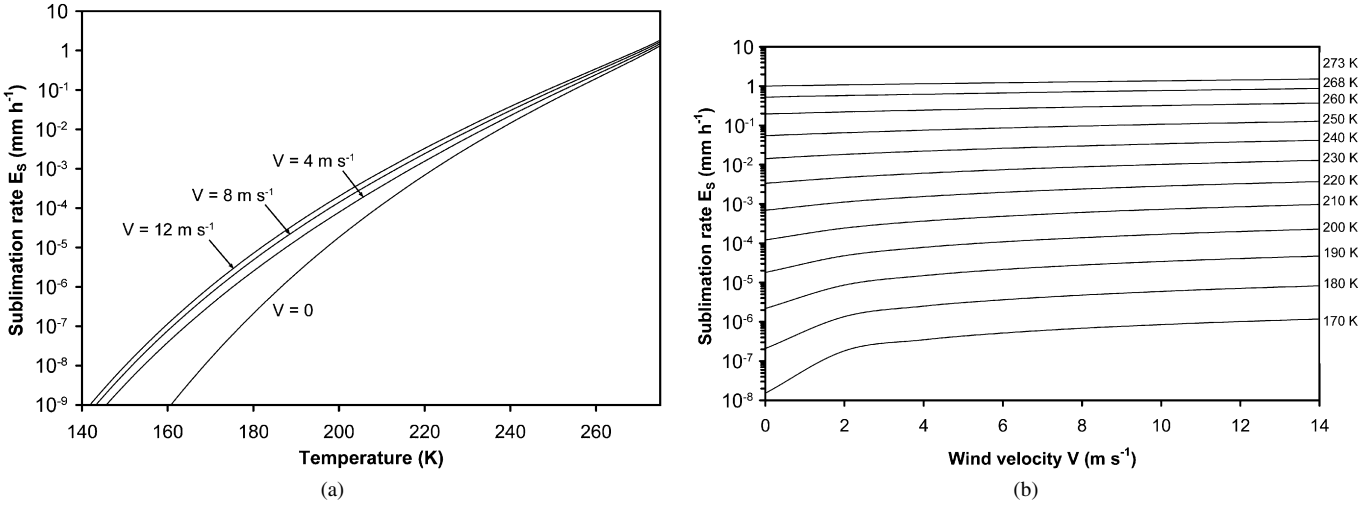

Fig. 8. Theoretical sublimation rate of water ice in martian conditions calculated using Eq. (22): (a) as a function of temperature for different wind velocities: 0, 4, 8 and 12 m s^{-1} and (b) as a function of the wind speed for various relevant temperatures. From these figures it is clear that the main control on the sublimation rate of ice on Mars is the temperature.

in the shallow surface of Mars, and eventually at the surface, in regions of higher latitude (Bandfield, 2007; Chevrier et al., 2007). Studying the effect of secondary parameters like wind or humidity becomes extremely important to characterize the timescale of ice presence on the surface.

5. Conclusions

Our experiments were designed to determine the effect of wind on the sublimation rate of water ice on the surface of Mars. In our low humidity experiments (Rh $\sim$ 1%), we observed an slow linear increase of the sublimation rate of ice for wind speeds ranging from 0 to 12 m s^{-1} at $-15\,^{\circ}$C and in our high humidity experiments (Rh $\sim$ 30%) no significant increase in sublimation rate with increasing wind speed could be detected. From our data we determined a semi-empirical equation that fully describes the sublimation of ice in the presence of free (buoyancy) and forced (wind) convection. However, contrary to previous suggestions, wind has only a very minor effect on the sublimation of ice. Amongst all studied parameters, temperature remains the most significant for the control of the sublimation rate of water ice (and also liquid water) on the martian surface.

Acknowledgments

We are grateful to Walter Graupner for laboratory assistance, as well as Rick Ulrich for discussions. We thank also Pr. Andrew Ingersoll and the anonymous reviewer for largely improving the quality of this manuscript. A major award from the W.M. Keck Foundation, Los Angeles, CA, supports the laboratory and present work.

References

Arpaci, V.S., Kao, S.H., 2001. Foundations of buoyancy driven heat transfer correlations. J. Heat Transfer 123, 1181–1184.

Bandfield, J.L., 2007. High-resolution subsurface water-ice distributions on Mars. Nature 447, 64–67.

Boynton, W.P., Brattain, W.H., 1929. Interdiffusion of gases and vapors. International Critical Tables 5.

Chevrier, V., Sears, D.W.G., Chittenden, J.D., Roe, L.A., Ulrich, R., Bryson, K., Billingsley, L., Hanley, J., 2007. The sublimation rate of ice under simulated Mars conditions and the effect of layers of mock regolith JSC Mars-1. Geophys. Res. Lett. 34, doi:10.1029/2006GL02840. L02203.

Churchill, S.W., Chu, H.H.S., 1975. Correlating equations for laminar and turbulent free convection from a vertical plate. Int. J. Heat Mass 18, 1323–1329.

Crane, 1988. Flow of fluids through valves, fittings, ans pipe. Technical Paper No. 410. Crane Company, Joliet, IL.

CRC, 2005–2006. CRC Handbook of Chemistry and Physics, 86th ed. CRC Press, Taylor & Francis Group, Boca Raton, FL.

Farmer, C.B., 1976. Liquid water on Mars. Icarus 28, 279–289.

Hecht, M.H., 2002. Metastability of liquid water on Mars. Icarus 156, 373–386.

Hess, S.T., Henry, R.M., Leovy, C.B., Ryan, J.A., Tillman, J.E., 1977. Meteorological results from the surface of Mars: Viking 1 and 2. J. Geophys. Res. 82, 4559–4574.

Hisatake, K., Tanaka, S., Aizawa, Y., 1993. Evaporation rate of water in a vessel. J. Appl. Phys. 73 (11), 7395–7401.

Hudson, T.L., Aharonson, O., Schorghofer, N., Farmer, C.B., Hecht, M.H., Bridges, N.T., 2007. Water vapor diffusion in Mars subsurface environments. J. Geophys. Res. 112 (E5), doi:10.1029/2006JE002815. E05016.

Ingersoll, A.P., 1970. Mars: Occurrence of liquid water. Science 168 (3934), 972–973.

Jakosky, B.M., Mellon, M.T., Varnes, E.S., Feldman, W.C., Boynton, W.V., Haberle, R.M., 2005. Mars low-latitude neutron distribution: Possible remnant near-surface water ice and a mechanism for its recent emplacement. Icarus 175, 58–67.

Kaydash, V.G., Kreslavskya, M.A., Shkuratova, Y.G., Videend, G., Bell, J.F., Wolff, M., 2006. Measurements of winds on Mars with Hubble Space Telescope images in 2003 opposition. Icarus 185 (1), 97–101.

Kays, W.M., Crawford, M.E., 1980. Convective Heat and Mass Transfer. McGraw–Hill, New York.

McAdams, W.H., 1954. Heat Transmission. McGraw–Hill, New York.

McQuiston, F.C., Parker, J.D., 1982. Heating, Ventilating, and Air Conditioning: Analysis and Design. Wiley, New York.

Mischna, M., Bell, J., James, P., Crisp, D., 1998. Synoptic measurements of martian winds using the Hubble Space Telescope. Geophys. Res. Lett. 25 (5), 611–614.

Moore, S.R., Sears, D.W.G., 2006. On laboratory simulation and the effect of small temperature oscillations about the freezing point and ice formation on the evaporation rate of water on Mars. Astrobiology 6 (4), 644–650.

Murphy, J.R., Leovy, C.B., Tillman, J.E., 1990. Observations of martian surface winds at the Viking Lander 1 site. J. Geophys. Res. 95, 14555–14576.

Popiel, C.O., Wojtkowiak, J., 2004. Experiments on free convective heat transfer from side walls of a vertical square cylinder in air. Exp. Therm. Fluid Sci. 29, 1–8.

Ryan, J.A., Sharman, R.D., Lucich, R.D., 1981. Local Mars dust storm generation mechanism. Geophys. Res. Lett. 8 (8), 899–901.

Schlichting, H., 1968. Boundary Layer Theory. McGraw–Hill, New York, pp. 252–310.

Schofield, J.T., Barnes, J.R., Crisp, D., Haberle, R.M., Larsen, S., Magalhaes, J.A., Murphy, J.R., Seiff, A., Wilson, G., 1997. The Mars Pathfinder Atmospheric Structure Investigation/Meteorology (ASI/MET) experiment. Science 278, 1752–1757.

Sears, D.W.G., Chittenden, J.D., 2005. On laboratory simulation and the temperature dependence of the evaporation rate of brine on Mars. Geophys. Res. Lett. 32. L23203.

Sears, D.W.G., Moore, S.R., 2005. On laboratory simulation and the evaporation rate of water on Mars. Geophys. Res. Lett. 32. L023443.

Sears, D.W.G., Roe, L.A., Moore, S.R., 2005. Stability of water and gully formation on Mars. Lunar Planet. Sci. XXXVI. 1496.

Sullivan, R., Greeley, R., Kraft, M., Wilson, G., Golombek, M., Herkenhoff, K., Murphy, J., Smith, P., 2000. Results of the Imager for Mars Pathfinder windsock experiment. J. Geophys. Res. 106 (E10), 24547–24562.

Wang, H., Ingersoll, A., 2003. Cloud-tracked winds for the first Mars Global Surveyor mapping year. J. Geophys. Res. 108 (E9). 5110.

Zarling, J.P., Braley, W.A., 1988. Geotechnical Thermal Analysis. Technical Council on Cold Regions Engineering Monograph, Embankment Design and Construction in Cold Regions, p. 48.

Zent, A.P., Haberle, R.M., Houben, H.C., Jakosky, B.M., 1993. A coupled subsurface-boundary layer model of water on Mars. J. Geophys. Res. 98 (E2), 3319–3337.